J. Plasma Physics (2015), *vol.* 81, 305810202 © Cambridge University Press 2014
doi:10.1017/S0022377814000956

Collisionless and collisional effects on plasma waves from a partition squeeze

Arash Ashourvan† and Daniel H. E. Dubin

Department of Physics, U.C. San Diego, La Jolla, CA 92093

(Received 18 June 2014; 11 September 2014; 3 October 2014; first published online 24 November 2014)

A simple 1D model is presented for the heating caused by cylindrically-symmetric plasma waves in a non-neutral plasma column due to the addition of a symmetric squeeze potential applied to the center of the column. We study this model by using analytical techniques and by using a numerical grids method solution, and we compare the results of this model to previous work (Ashourvan and Dubin (2014)). squeeze divides the plasma into passing and trapped particles; the latter cannot pass over the squeeze potential. In collisionless theory, enhanced heating is caused by additional bounce harmonics induced by the squeeze in the particle distribution, leading to Landau resonances at energies E_n for which the bounce frequency $\omega_b(E)$ and wave frequency ω_m satisfy $\omega_m = n\omega_b(E_n)$. As a result, heating is substantially higher than the case with no squeeze, even when ω_m is much greater than the thermal bounce frequency $\omega_b(T)$. Adding collisions to the theory creates a boundary layer at the separatrix between trapped and passing particles that further enhances the heating at small $\omega_m/k_m v_s$, where k_m is the axial wavenumber and v_s is the velocity at the separatrix. However, at large ω_m/v_s, the heating from the separatrix boundary layer is only a small correction to the heating from collisionless resonances in the trapped particle distribution function.

1. Introduction

Trivelpiece–Gould (TG) modes are electrostatic normal modes of a cylindrical plasma column [Trivelpiece and Gould (1959)]. In this paper, we study the plasma heating (and associated wave damping) caused by cylindrically-symmetric Trivelpiece–Gould modes with frequency ω_m and axial wave number k_m, after applying a cylindrically-symmetric 'squeeze' potential to the plasma equilibrium. Without the squeeze, the heating is caused by Landau damping of the wave energy, due to resonant particles with axial velocity v equal to the wave phase velocity ω_m/k_m. With the squeeze, the heating is enhanced because new resonances appear in the velocity distribution. The new resonances occur because the squeeze potential changes the particle orbits, creating a non-sinusoidal time-dependence for the wave as seen in the particle frame, which induces new resonances at harmonics of the particle bounce frequency ω_b, i.e. where $\omega_m = n\omega_b(E)$ for integer n (where E is the particle kinetic energy).

This effect was studied in a previous paper (Ashourvan and Dubin 2014), where it was shown that the enhanced heating scales as the square of the applied squeeze potential φ_s for small squeeze, provided that the wave phase velocity is large

† Email address for correspondence: ddubin@ucsd.edu

https://doi.org/10.1017/S0022377814000956 Published online by Cambridge University Press

compared to the thermal speed $v_T = \sqrt{T/m}$. Otherwise, the wave damping is dominated by standard Landau damping and is largely independent of squeeze for small squeeze; see Fig. 3 of the reference. However, in order to formulate a general theory that fully accounts for the effects of radial inhomogeneity in the plasma, several simplifying approximations were made. First, collisional effects on the mode damping were neglected. Second, the squeeze potential, while allowed to have a general functional form in radius and axial position, was treated as a small perturbation, and consequently particles trapped by the squeeze were neglected. A squeeze potential with maximum magnitude φ_s traps particles to the left and right of the squeeze if their velocities satisfy $|v| < v_s$, where the separatrix velocity v_s is defined as

$$\varphi_s = \frac{1}{2} m_q v_s^2. \tag{1}$$

The resulting theory was tested against collisionless numerical simulations that kept trapped particle effects and finite squeeze amplitude (but neglected radial inhomogeneity for simplicity), and good agreement between the simulations and theory for both the damping rate and the frequency shift to the modes was found for small applied squeeze potentials, $\varphi_s/T < 1$.

However, in this paper we show that trapped particle effects on the enhanced mode damping due to applied squeeze can be significant, and we describe the conditions under which they can be neglected. We include collisional and trapped particle effects on the squeeze damping of TG modes via a simplified 1D model of the system. For simplicity the model neglects radial inhomogeneity as well as collective shielding of the potentials, but includes enough physics in order to provide some insight into the contributions of trapped particles and collisions to the wave damping. The model treats the squeeze as an infinitesimally narrow reflecting potential that partitions low energy particles on the left and right side of the plasma, without assuming that the magnitude of the potential is a small perturbation. The model includes the effect of weak collisions via a Fokker–Planck collision operator.

We find that, for small squeeze and large phase velocity, this model yields enhanced wave damping due to squeeze with the same square dependence on the applied squeeze potential as in Ashourvan and Dubin (2014). However, trapped particles dominate the squeeze damping as opposed to the results obtained in Ashourvan and Dubin (2014). We estimate under what conditions trapped particles can be neglected when evaluating the enhanced damping caused by squeeze, and we find that these conditions were satisfied in the examples studied in Ashourvan and Dubin (2014).

Finally, the model shows that collisions can further enhance the wave damping due to a boundary layer at the separatrix between passing and trapped particles that is created by the partition squeeze. Trapped particles respond differently to the drive potential than passing particles and consequently a discontinuity in the particle distribution function develops at the separatrix velocity. Collisions smooth out the discontinuity, creating a boundary layer of width proportional to $\sqrt{\nu}$ where ν is the collision frequency, and causing heating proportional to $\sqrt{\nu}$. This enhanced collisional boundary layer heating has been shown to lead to strongly enhanced damping and particle transport for various types of waves (Hilsabeck and O'Neil 2003; Kabantsev and Driscoll 2006; Dubin and Tsidulko 2011; Driscoll et al. 2013). For small ν/ω_m the boundary layer damping effect is much larger than viscous damping due to collisions (Anderson and O'Neil 2007) which scales like ν rather than $\sqrt{\nu}$.

https://doi.org/10.1017/S0022377814000956 Published online by Cambridge University Press

Surprisingly, however, we find that this boundary layer collisional enhancement effect is only important for low phase velocities, $\omega_m/k_m v_s < 1$. In the opposite regime $\omega_m/k_m v_s > 1$ (the regime of interest in most TG wave damping experiments) we find that the discontinuity between trapped and passing particles becomes small, and thus the collisional heating becomes negligible. The discontinuity vanishes at large phase velocities because the particle response to a wave of high-frequency compared to the bounce frequency becomes independent of whether the particles are trapped or passing.

In Sec. 2, we introduce our 1D slab geometry plasma model. We apply a small standing sinusoidal (in both space and time) drive potential with angular frequency ω_m to the plasma and obtain the linear distribution function of a collisionless plasma in response to the drive potential. In Sec. 3, we evaluate the resonant plasma heating. We find that the trapped particles moving in z experience a non-sinusoidal mode potential caused by the squeeze, producing high-frequency harmonics that can resonate with the wave frequency to cause Landau damping and satisfy the condition $\omega_b(E_n) = \omega_m/n$, where $\omega_b(E)$ is the frequency of axial bounce motion of particles with energy E, even when the mode phase velocity is large compared to the thermal velocity. We will see that these added resonances cause an enhancement to the plasma heating rate that has a $|\varphi_s|^2$ dependence.

In Sec. 4, we add weak collisions to the system in the form of a Fokker–Planck collision operator. Due to the discontinuities at the separatrix, the velocity derivatives of this collision operator are large in this region. Using the boundary layer method we obtain a local solution to the distribution function at the separatrix which has a width proportional to $\sqrt{D}$, where D is the velocity diffusion coefficient (proportional to the collision frequency). The boundary layer connects and smooths out the discontinuities present in the collisionless theory. We evaluate the heating in the separatrix layer and compare our analytical results to the heating evaluated from the numerical grids method.

2. 1D model

In the plasma model presented here, we neglect radial variation for simplicity, we assume the plasma ends are flat, and that particles undergo specular reflection at the ends, $z = \pm L/2$ where L is the length of the plasma column. We also assume that the squeeze potential is symmetric in z with respect to the center of plasma. This is not necessarily the case in the experiments, however this added symmetry simplifies the problem. To further simplify the analysis we also assume that the squeeze potential is narrow in z, taking it to be non-zero only at $z = 0$. Thus particles with velocities satisfying $|v| < v_s$ undergo specular reflection from the squeeze, whereas particles with $|v| > v_s$ are unaffected by it.

In our 1D model, collisionless plasma dynamics is described by the time evolution of the 1D Vlasov equation

$$\frac{\partial f}{\partial t} + v\frac{\partial f}{\partial z} - \frac{1}{m_q}\frac{\partial \delta\varphi}{\partial z}\frac{\partial f}{\partial v} = 0\,, \tag{2}$$

where $f(z, v, t)$ is the particle distribution function, $\delta\varphi(z, t)$ is the wave potential. Due to the reflective boundary conditions, the distribution function must satisfy the

https://doi.org/10.1017/S0022377814000956 Published online by Cambridge University Press

following conditions:

$$f(\pm L/2, v) = f(\pm L/2, -v) \quad \text{at the plasma ends,} \tag{3}$$

$$f(0, v) = f(0, -v) \quad \text{at the squeeze, for trapped particles only.} \tag{4}$$

For a long thin plasma to the lowest order in $\omega_m/\omega_p \ll 1$, the boundary conditions on the wave potential at the axial ends of plasma are $\partial_z \delta\phi(\pm L/2) \approx 0$ (Prasad and O'Neil 1983). Therefore, we take the wave potential $\delta\varphi(z, t)$ to be in the form of a standing wave as follows:

$$\delta\varphi(z, t) = |\delta\overline{\phi}| \cos[k_m(z + L/2)] \cos[\omega_m t - \alpha_0] \tag{5}$$

$$= \delta\phi(z) e^{-i\omega_m t} + \delta\phi^*(z) e^{i\omega_m t}, \tag{6}$$

where $k_m \equiv \pi m/L$,

$$\delta\phi(z) = \tfrac{1}{2}\delta\overline{\phi} \cos[k_m(z + L/2)], \tag{7}$$

and $\delta\overline{\phi} = |\delta\overline{\phi}| e^{i\alpha_0}$. Note that this single-mode spatial form for the wave potential does not include self-consistent effects produced by the squeeze: in a self-consistent approach the squeeze potential changes the spatial form of the normal modes. This effect was considered in Ref. Ashourvan and Dubin (2014), where it was shown to produce an extra collisionless heating term. We neglect this self-consistent effect here for simplicity, as we are interested in resonance and collisional effects unrelated to the self-consistent potential terms.

For a small amplitude wave in the linear approximation the particle distribution is given by

$$f(z, v, t) = n_0(\mathrm{F}_0(v) + \delta\mathrm{f}(z, v, t)) . \tag{8}$$

Here, n_0 is the density of a uniform neutralizing background charge (provided by rotation at a given frequency through the uniform magnetic field in the actual plasma system). The term $n_0\mathrm{F}_0(z, v)$ is the equilibrium distribution function and δf is the perturbed distribution function due to the presence of the wave. The perturbed distribution has the following form:

$$\delta\mathrm{f}(z, v, t) = \delta f(z, v) e^{-i\omega_m t} + \delta f^*(z, v) e^{i\omega_m t}. \tag{9}$$

We choose the equilibrium distribution to be of the Boltzmann type:

$$\mathrm{F}_0(v) = \frac{\exp[-m_q v^2/2T]}{\sqrt{2\pi T/m_q}}, \tag{10}$$

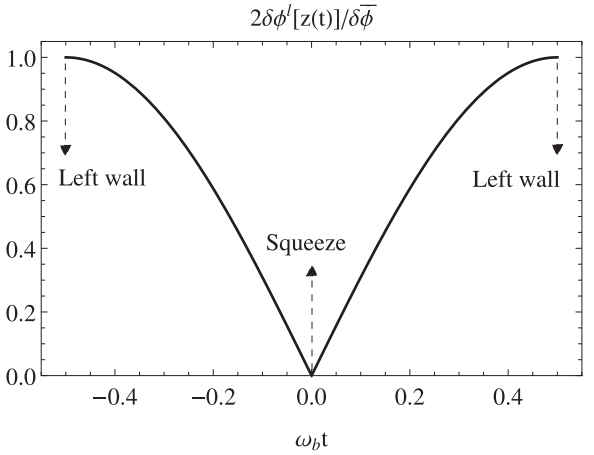
normalized such that

$$\int_{-\infty}^{\infty} \int_{-L/2}^{L/2} \mathrm{F}_0 dv dz = 1 . \tag{11}$$

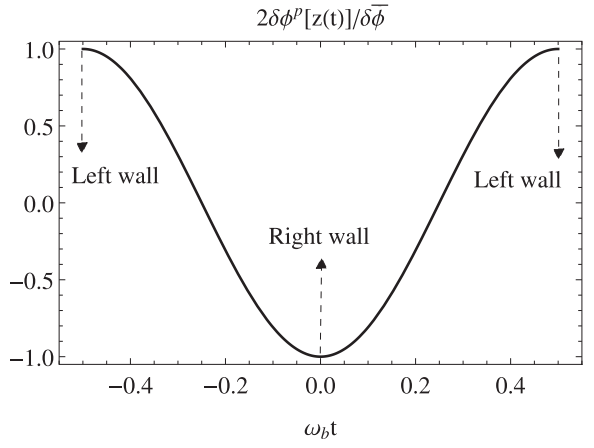
The presence of the squeeze is implicit in the (10): the function does not show a spatial (z) dependence, however the squeeze potential is built into the distribution function and particles with velocities $|v| < v_s$ are trapped and have different unperturbed orbits than the passing particles. Thus δf must be solved separately for trapped and passing particles. For a small amplitude perturbation we linearize the Vlasov equation to obtain:

$$\frac{\partial \delta\mathrm{f}}{\partial t} + v\frac{\partial \delta\mathrm{f}}{\partial z} + v\frac{\partial \delta\varphi}{\partial z}\frac{\mathrm{F}_0}{T} = 0 , \tag{12}$$

https://doi.org/10.1017/S0022377814000956 Published online by Cambridge University Press



(a)



(b)

FIGURE 1. Plots of the potentials experienced by a left-trapped (Fig. 1(a)) and a passing (Fig. 1(b)) particle along their unperturbed orbits.

where we used $\partial_v F_0 = -m_q v F_0/T$. We want to use Fourier series expansion to solve for δf, however all the boundaries are of the reflective type. For a mode with odd mode number m [see (5)] we see that trapped particles experience a non-sinusoidal potential. Figures 1(a) and (b), respectively depict the potential experienced by a left-trapped and a passing particle along their unperturbed orbit. Here $z(t)$ is the position of a particle as a function of time, moving at a constant speed $|v|$ (in its unperturbed orbit). The potential for passing particles is a cosine and the particle's bounce orbiting motion is identical to the motion of a particle moving at a constant velocity, along an extended coordinate, under a periodic cosine potential. For trapped particles this is obviously not the case and the potential (for odd m) as seen by the particle is not of a cosine form.

We can convert these specular reflection boundary conditions into periodic boundary conditions by even periodic extension of the phase space. This is done

https://doi.org/10.1017/S0022377814000956 Published online by Cambridge University Press

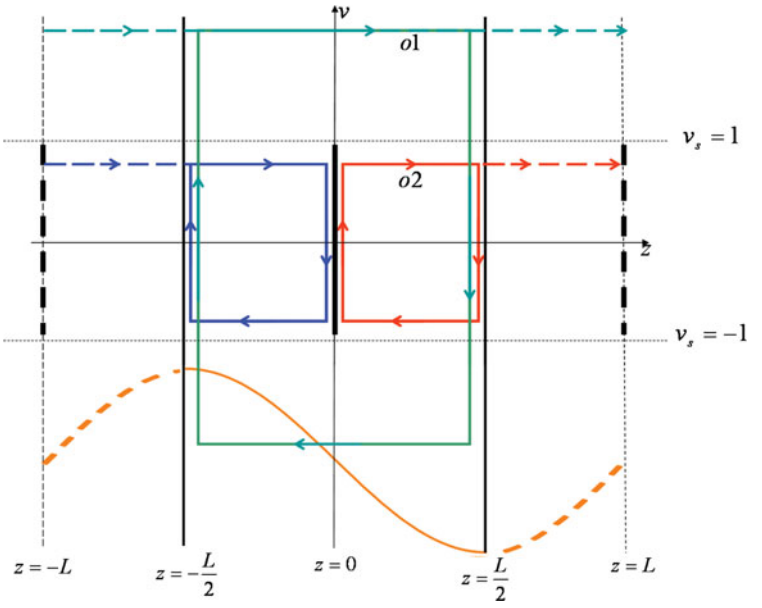


FIGURE 2. A schematic description of extension of the phase space. The sinusoidal curve at the bottom of the figure is the wave potential. The solid part of the plot is inside the original system and the dashed part is a portion of the extended region.

by removing the reflecting walls and replacing them with the mirror image of half of the phase space with respect to that wall. A schematic description of this method is given in Fig. 2. An arbitrary passing particle would travel along orbit $o1$ in phase space, along which it would reflect off of the right wall and instantly go to negative velocity space and then moves in the negative direction. Now with the new boundary conditions, where there are no walls and the wave potential has been extended (an even periodic extension) and phase space is periodically extended as well, that specific passing particle will move to the right side of $z = L/2$ where the right wall used to be, and it will move along until it reaches $z = L$. At this point it will disappear and reappear at $z = -L$. In the extended part of phase space particle will see the same potential as it would have originally, in the infinite wall case.

A particle in the right trap would travel to the right along orbit $o2$, reflect off of the wall at $z = L/2$ and move to left in the negative velocity space until it hits the squeeze and reflects again and moves to right in positive velocity space. Now with the periodic boundary condition, trapped particle moves to the right side of $z = L/2$ until it reaches the image of the squeeze at $z = L$, there it disappears and Then reappears at the position of the actual squeeze at $z = 0$ and again moves to the right. Notice that with this type of boundary conditions, a particle's velocity does not change sign and particles keep moving in the same direction. Hence the new boundary conditions on δf are

$$\delta f(z + 2L, v) = \delta f(z, v), \quad \text{passing} \tag{13}$$

$$\delta f(z + L, v) = \delta f(z, v), \quad \text{left trap} \tag{14}$$

$$\delta f(z + L, v) = \delta f(z, v), \quad \text{right trap} \tag{15}$$

https://doi.org/10.1017/S0022377814000956 Published online by Cambridge University Press

Similarly, the potential has periodic extensions. For passing particles the extended potential is defined on $-L \leqslant z \leqslant L$, has period $2L$, and is sinusoidal:

$$\delta\varphi^p(z,t) = \delta\phi^p(z)e^{-i\omega_m t} + (\delta\phi^p(z))^* e^{i\omega_m t} \tag{16}$$

$$\delta\phi^p(z) = \tfrac{1}{2}\delta\overline{\phi}\cos[k_m(z+L/2)], \quad -L \leqslant z \leqslant L; \quad \delta\phi^p(z+2L) = \delta\phi^p(z)$$

$$\delta\phi^p(z) = \delta\phi^p_m e^{ik_m(z+L/2)} + \delta\phi^p_{-m} e^{-ik_m(z+L/2)}, \quad \delta\phi^p_m = \frac{1}{4}\delta\overline{\phi}. \tag{17}$$

For the left trap the potential is defined over $-L \leqslant z \leqslant 0$ and its periodic extension is periodic with period L:

$$\delta\varphi^l(z,t) = e^{-i\omega_m t}\delta\phi^l(z) + e^{i\omega_m t}(\delta\phi^l(z))^*, \tag{18}$$

where

$$\delta\phi^l(z) = \tfrac{1}{2}\delta\overline{\phi}\cos[k_m(z+L/2)], \quad -L \leqslant z \leqslant 0; \quad \delta\phi^l(z+L) = \delta\phi^l(z). \tag{19}$$

For the right trap the potential is defined over $0 \leqslant z \leqslant L$ and its periodic extension is also periodic with period L:

$$\delta\varphi^r(z,t) = e^{-i\omega_m t}\delta\phi^r(z) + e^{i\omega_m t}(\delta\phi^r(z))^* \tag{20}$$

$$\delta\phi^r(z) = \tfrac{1}{2}\delta\overline{\phi}\cos[k_m(z+L/2)], \quad 0 \leqslant z \leqslant L; \quad \delta\phi^r(z+L) = \delta\phi^r(z). \tag{21}$$

The trapped potentials can be expanded as a Fourier series with periodicity L. For the left potential,

$$\delta\phi^l(z) = \sum_{n=-\infty}^{\infty} \delta\phi^l_n e^{ik_{2n}z} \tag{22}$$

$$\delta\phi^l_n = \tfrac{1}{2}\delta\overline{\phi}C^l_n, \quad C^l_n = \frac{1}{\delta\overline{\phi}L}\int_{-L}^{0} \delta\phi^l(z)e^{-ik_{2n}z}dz, \tag{23}$$

while for the right potential (assuming m is odd),

$$\delta\phi^r(z) = -\delta\phi^l(z). \tag{24}$$

Using (19) and (23) the coefficients C^l_n can be evaluated:

$$C^l_n = \frac{2k_m}{k_m^2 - k_{2n}^2}\sin\left[\tfrac{k_m}{2}\right] \tag{25}$$

$$C^r_n = -C^l_n \tag{26}$$

We can use these extensions to solve the linearized Vlasov equation, (12). For the passing particles, the solution compatible with boundary conditions (13) and the potential given by (16) and (17) is of the form

$$\delta\mathrm{f}^p(z,v,t) = e^{-i\omega_m t}\delta f^p(z,v) + c.c. \tag{27}$$

$$\delta f^p(z,v) = \delta f^p_m(v)e^{ik_m(z+L/2)} + \delta f^p_{-m}(v)e^{-ik_m(z+L/2)}. \tag{28}$$

Substituting in (12) we obtain,

$$-i\omega_m\delta f^p_m + ivk_m\delta f^p_m + ik_m v\delta\phi^p_m\frac{\mathrm{F}_0}{T} = 0. \tag{29}$$

Solving for δf^p_m yields

$$\delta f^p_m = \frac{v\delta\phi^p_m \mathrm{F}_0/T}{\omega_m/k_m - v}. \tag{30}$$

https://doi.org/10.1017/S0022377814000956 Published online by Cambridge University Press

The position and velocity dependence of the distribution function is then given by:

$$\delta f^{p}(z, v) = \frac{v\delta\phi^{p}_{m}\mathrm{F}_0/T}{\omega_m/k_m - v}e^{ik_m(z+L/2)} + \frac{v\delta\phi^{p}_{-m}\mathrm{F}_0/T}{-\omega_m/k_m - v}e^{-ik_m(z+L/2).} \tag{31}$$

On the other hand, for the trapped particles the distribution function compatible with (14) or (15) and potentials (22) or (24) are

$$\delta\mathrm{f}^{l(r)}(z, v, t) = e^{-i\omega_m t}\delta f^{l(r)}(z, v) + c.c. \tag{32}$$

$$\delta f^{l(r)}(z, v) = \sum_{n=-\infty}^{\infty} \delta f^{l(r)}_{n}(v)e^{ik_{2n}z} \tag{33}$$

In the above sums the $n = 0$ term is excluded, since in linear theory the average density in the left trap and right trap does not change. For left trapped particles the linearized Vlasov (12) then implies that

$$\delta f^{l}_{n} = \frac{v\delta\phi^{l}_{n}\mathrm{F}_0/T}{\omega_m/k_{2n} - v} \tag{34}$$

The position and velocity dependence of the trapped distribution function is given by:

$$\delta f^{l(r)}(z, v) = \sum_{n=-\infty}^{\infty} \frac{v\delta\phi^{l(r)}_{n}\mathrm{F}_0/T}{\omega_m/k_{2n} - v}e^{ik_{2n}z} \tag{35}$$

Figure 3 depicts the position and velocity dependence of the perturbed distribution function for trapped and passing particles at the separatrix velocity ($v = v_s$), evaluated from (31) and (35) respectively. The plotted function $(\delta f/\delta\phi)/(F_0/T)$ is a function of the dimensionless parameter ω_m/k_1v_s. The distribution function δf is discontinuous at the separatrix. This discontinuity is unphysical and is an artifact of treating the plasma as a collisionless system. Adding collisions to the system will allow particle interchange between the trapped and passing regions and as a result, the solutions for δf at the separatrix will connect and smooth out. In the next section we will add a weak collison operator and solve for the distribution function of the collisional system at the separatrix region.

Furthermore, in Fig. 4 we can see many singularities present in the trapped region. These singularities are located in velocities $v = \omega_m/k_{2n}$, in the trapped region of phase space $(-v_s < v < v_s)$, corresponding to velocities in resonance with the drive potential. The distribution of the resonant particles can be obtained by adding a small collision term to the Vlasov equation $(-\nu\delta\mathrm{f})$, and applying the Plemelj formula to the relations (30) for passing particles and (34) for the trapped particles:

$$\lim_{\nu\to 0}\delta f^{l(r)}_{n} = \mathrm{P}\frac{v\delta\phi^{l(r)}_{n}\mathrm{F}_0/T}{\omega_m/k_{2n} - v} - i\pi\delta(v - \omega_m/k_{2n})v\delta\phi^{l(r)}_{n}\mathrm{F}_0/T \tag{36}$$

$$\lim_{\nu\to 0}\delta f^{p}_{m} = \mathrm{P}\frac{v\delta\phi^{p}_{m}\mathrm{F}_0/T}{\omega_m/k_m - v} - i\pi\delta(v - \omega_m/k_m)v\delta\phi^{p}_{m}\mathrm{F}_0/T \tag{37}$$

This treatment is equivalent to integrating along the Landau contour, i.e. dropping below the poles (Krall and Trivelpiece 1986). In (36) and (37) the first term gives the distribution of the non-resonant particles and 'P' represents the principal value of the argument. The imaginary parts give the distribution of the resonant population, which in the collisionless theory has zero width and is given by the Dirac delta function.

https://doi.org/10.1017/S0022377814000956 Published online by Cambridge University Press

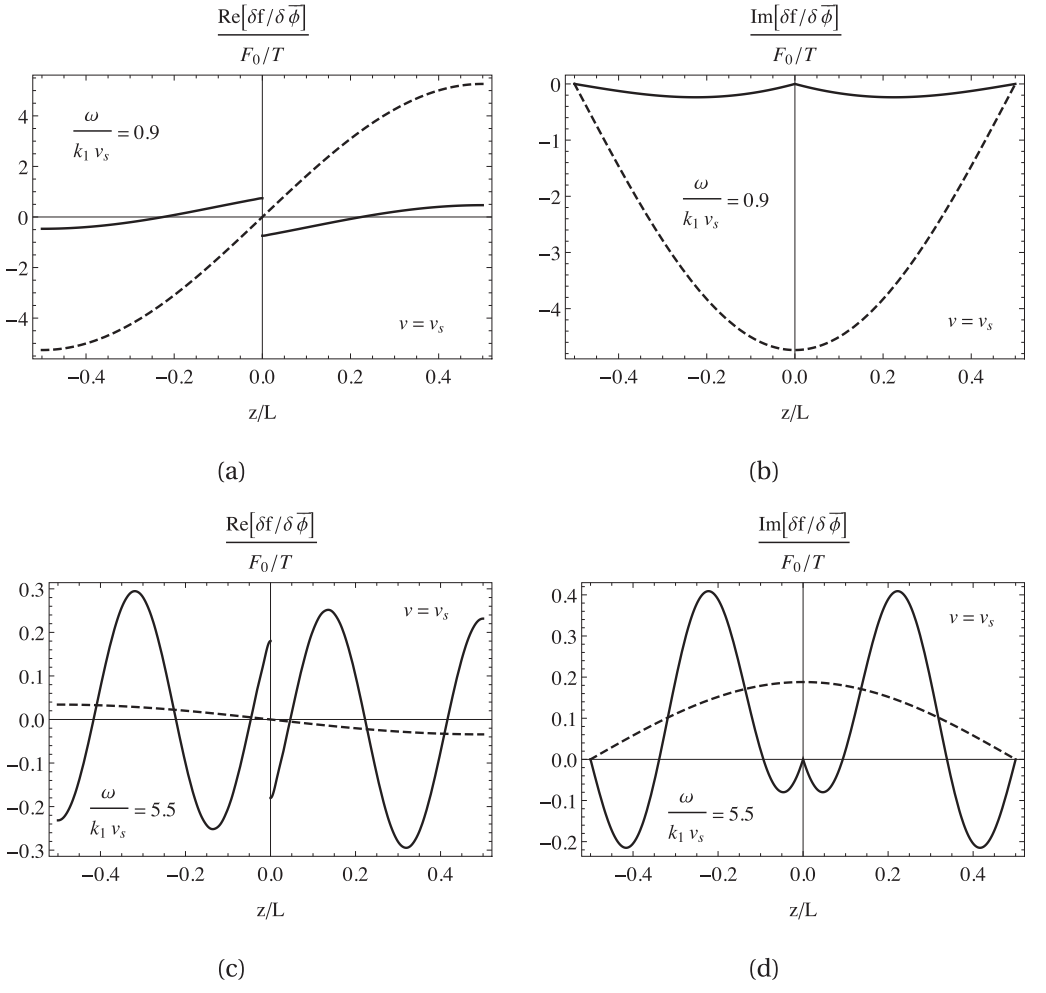


FIGURE 3. Plots of δf as a function of z for the trapped (solid) and passing (dashed) particles at the separatrix ($v = v_s$), using (31) and (35) respectively.

The drive potential performs work on the resonant particles which will result in the heating of the plasma.

3. Collisionless heating

The wave performs work on particles as they move along their (unperturbed) orbits. The time averaged heating of particles over one period of external force is obtained by integrating over the whole phase space accessible to particles, which is

$$\left\langle \frac{dE}{dt} \right\rangle_t = n_0 \frac{\omega}{2\pi} \int_0^{2\pi/\omega} dt \int_{-L/2}^{L/2} \int_{-\infty}^{\infty} dz v dv \delta \mathrm{f}(z, v, t) \left(-\partial_z \delta\varphi(z, t)\right)$$
$$= -n_0 \int_{-L/2}^{L/2} \int_{-\infty}^{\infty} dz v dv \left[\delta f(z, v) \partial_z \left(\delta\phi(z)\right)^* + \delta f^*(z, v) \partial_z \delta\phi(z)\right] \qquad (38)$$

https://doi.org/10.1017/S0022377814000956 Published online by Cambridge University Press

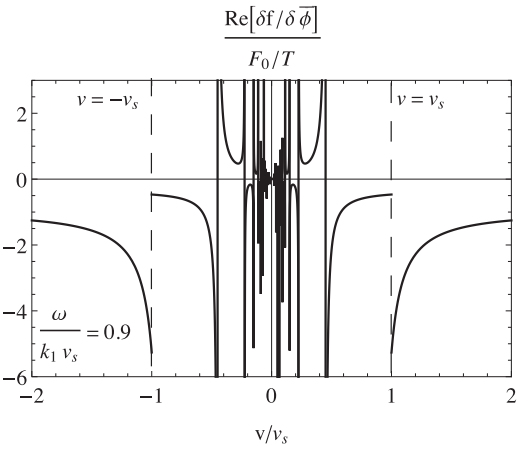


FIGURE 4. Real part of the perturbed distribution function versus velocity using (31) and (35) respectively, for the drive frequency $\omega_m/k_1 v_s = 0.9$, at $z = -L/2$.

We break the integration over the entire phase space to integrations over the passing and trapped regions:

$$\left\langle \frac{dE}{dt} \right\rangle_t =$$
$$-n_0 \int_{-L/2}^{L/2} \left(\int_{v_s}^{\infty} + \int_{-\infty}^{-v_s} \right) dz v dv \left[\delta f^p(z,v) \partial_z \left(\delta\phi^p(z)\right)^* + \left(\delta f^p(z,v)\right)^* \partial_z \delta\phi^p(z) \right]$$
$$-n_0 \int_{-L/2}^{0} \int_{-v_s}^{v_s} dz v dv \left[\delta f^l(z,v) \partial_z \left(\delta\phi^l(z)\right)^* + \left(\delta f^l(z,v)\right)^* \partial_z \delta\phi^l(z) \right]$$
$$-n_0 \int_{0}^{L/2} \int_{-v_s}^{v_s} dz v dv \left[\delta f^r(z,v) \partial_z \left(\delta\phi^r(z)\right)^* + \left(\delta f^r(z,v)\right)^* \partial_z \delta\phi^r(z) \right]$$

Using (28), (33), (22) and (17) in (39), only the resonant particles are heated and have a non-zero contribution to $\left\langle \frac{dE}{dt} \right\rangle_t$ which results in:

$$\left\langle \frac{dE}{dt} \right\rangle_t = \pi L n_0 \frac{|\delta\bar{\phi}|^2}{T} \left(\frac{k_m}{4} \Theta[\omega_m/k_m - v_s] v^2 \mathrm{F}_0(v)|_{v=\frac{\omega}{k_m}} + \sum_{n=n_{\min}}^{\infty} k_{2n} |C_n^l|^2 v^2 \mathrm{F}_0(v)|_{v=\frac{\omega}{k_{2n}}} \right), \quad n_{\min} = \lceil \tfrac{\omega}{k_2 v_s} \rceil. \tag{39}$$

In the above equation $\Theta[x]$ is the step function defined as

$$\Theta[x] = 1, \quad x > 0, \qquad = 0, \quad x \leqslant 0. \tag{40}$$

Furthermore, $\lceil x \rceil$ is the ceiling function, defined as the greater integer between two integers which are the closest to the real number x. In (39), the first term on the right-hand side corresponds to the average work per unit time, performed on the passing particles in resonance with the drive potential. There is only a single resonance related to the passing particles and this resonance only can exist for frequencies $\omega > k_m v_s$.

The second term on the right-hand side of (39) corresponds to the average work per unit time performed on all the trapped particles. Because of the symmetry of the

https://doi.org/10.1017/S0022377814000956 Published online by Cambridge University Press

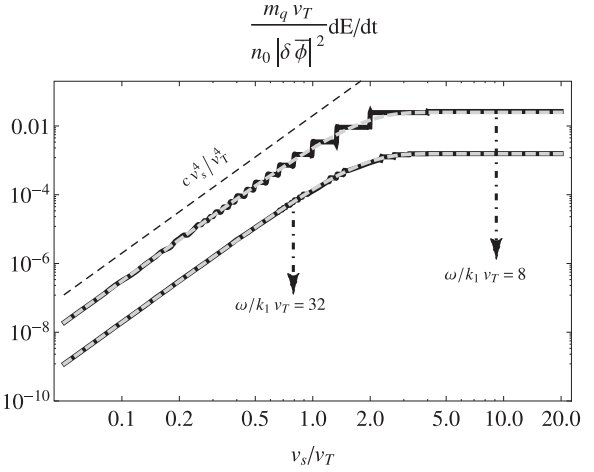


FIGURE 5. Heating power of a collisionless plasma from (39) for large phase velocities $\omega_m/k_1 v_T = 8$ and $\omega_m/k_1 v_T = 32$, for mode $m = 1$. The straight dashed line depicts an arbitrary v_s^4/v_T^4 dependence, for comparison. The dashed curves on top of the solid lines are approximate solutions given by (A 8).

wave potential and the squeeze, left trap and right trap heating has the same average value. The sum is over all the resonances between the trapped particles and the wave potential. The reason for the presence of a series of resonances is that the potential as seen by the particles is non-sinusoidal and contains a series of harmonics which are at resonance with the wave potential at the velocities

$$v_n = \frac{\omega}{k_{2n}}, \quad n = 1, 2, \ldots \tag{41}$$

This equation implies that the higher the number n of the resonance, the lower is the velocity of the particles in that resonance. Moreover, the nth resonance cannot exist for $v_n > v_s$, which is reflected in the plot of the heating versus v_s/v_T in Fig. 5: lowering v_s at a constant ω_m results in instant, discontinuous drops of heating, which happens each time a trapped resonance disappears at the separatrix. The lower bound of the sum is given by the highest velocity in the trapped region which is in resonance with the drive potential and is located at the velocity

$$v_{n_{\min}} = \frac{\omega}{k_{2n_{\min}}}. \tag{42}$$

To facilitate comparison with previous work on damping of TG modes, we note that the mode damping rate γ_m can be obtained from the heating rate via the equation (Stix 1962)

$$\gamma_m = \left\langle \frac{dE}{dt} \right\rangle_t / 2E_m, \tag{43}$$

where E_m is the mode energy. The total energy in an electrostatic plasma normal mode is also found in Ref. Stix (1962):

$$E_m = \frac{1}{16\pi q^2} \int dz\, \nabla\delta\phi^* \cdot \left(\frac{\partial}{\partial\omega_m}(\omega_m \mathbf{K}_h) \right) \cdot \nabla\delta\phi, \tag{44}$$

where $\mathbf{K}_h$ is the Hermitian part of the dielectric tensor associated with the waves (and we note that our perturbed potential has units of energy not voltage). The dielectric

https://doi.org/10.1017/S0022377814000956 Published online by Cambridge University Press

tensor for TG modes in a 1D Maxwellian plasma is given by the expression

$$\mathbf{K} = \mathbf{1} - \frac{\hat{z}\hat{z}\omega_p}{\sqrt{2\pi}k_m\lambda_D}\int dv \frac{ve^{-v^2/2}}{\omega_m - k_m v_T v}. \tag{45}$$

After some work, assuming uniform density and using (5) for the mode potential, this allows us to write the mode energy as

$$E_m = \frac{Ln_0}{8\sqrt{2\pi}}\frac{|\delta\overline{\phi}|^2}{T}\frac{\omega_m}{k_m v_T} P\int \frac{ve^{-v^2/2}}{(\omega_m/k_m v_T - v)^2}dv. \tag{46}$$

In the high phase velocity regime of weak wave damping $\omega_m/k_m v_T \gg 1$, the energy simplifies to

$$E_m = \frac{Ln_0 k_m^2}{4m_q\omega_m^2}|\delta\overline{\phi}|^2. \tag{47}$$

Using (43) and (47), the first term in (39) leads to the usual Landau damping rate for an unsqueezed plasma column; see for example (4) of Danielson and Anderegg 2004. This expression also agrees with the unsqueezed rate γ_0 derived in Ashourvan and Dubin 2014. The second term in (39) is due to particles trapped by the squeeze interacting with the wave potential. This effect is not included in Ashourvan and Dubin 2014, which neglects trapped particles. If Eq. (106) of Ashourvan and Dubin 2014 is evaluated for a partition squeeze of the type considered here, the squeeze damping rate γ_2 due to passing particles vanishes because *all* Fourier components of the squeeze vanish (a partition squeeze is a type of singular function that has no Fourier representation). This agrees with (39), which also shows passing particles do not contribute to the squeeze damping for a partition squeeze.

For low phase velocities such that $\omega_m/k_m < v_s$ and $n_{\min} = 1$, the heating equation will have the following functional form:

$$\left\langle \frac{dE}{dt} \right\rangle_t = \pi L n_0 \frac{|\delta\overline{\phi}|^2}{T}\sum_{n=1}^{\infty} k_{2n}|C_n^m|^2 v^2 \mathrm{F}_0(v)|_{v=\frac{\omega}{k_{2n}}}. \tag{48}$$

Therefore, in this small phase velocity limit the collisionless plasma heating is independent of the size of the squeeze (v_s).

On the other hand, in the high phase velocity regime $\omega_m/k_m v_T \gg 1$, the heating due to the passing resonance becomes exponentially small, because of the F_0 term in (39). However, heating of the trapped particles consists of many resonances for which F_0 is not exponentially small. As a result, trapped particle heating is finite even for $\omega_m/k_m v_T \gg 1$. The functional form of the heating due to trapped particles depends on v_s/v_T. As we can see from the Fig. 5 for $v_s/v_T \gg 1$ the plasma heating is independent of v_s/v_T, since plasma is practically cut in half and further raising v_s is not going to change the plasma configuration. On the other hand, in the limit $v_s/v_T \ll 1$, the sum of the large number of resonances results in a v_s^4 dependence for the plasma heating. We have derived these functional forms in Appendix A, which yielded the following results:

$$\frac{dE^t}{dt} = \frac{2n_0|\delta\overline{\phi}|^2}{m_q}\sqrt{\frac{2}{\pi}}\frac{v_T}{(\omega_m/k_m)^2}, \quad \tfrac{\omega_m}{k_m v_T} \gg \tfrac{v_s}{v_T} \gg 1 \tag{49}$$

$$= \frac{n_0|\delta\overline{\phi}|^2}{4m_q}\sqrt{\frac{2}{\pi}}\frac{v_s^4}{(\omega_m/k_m)^2 v_T^3}, \quad \tfrac{\omega_m}{k_m v_T} \gg 1 \gg \tfrac{v_s}{v_T} \tag{50}$$

https://doi.org/10.1017/S0022377814000956 Published online by Cambridge University Press

The small squeeze form of the heating given by (50), when combined with (43) and (47), yields a mode damping rate that has the same scaling with squeeze potential (i.e. proportional to φ_s^2) as was found in (106) of Ashourvan and Dubin 2014. However, this trapped particle term was not included in Ashourvan and Dubin (2014), which includes only passing particles. Furthermore, in Ashourvan and Dubin (2014) a comparison of the damping calculation to simulations that kept trapped particles showed good agreement over a range of squeeze amplitudes (see Fig. 3 of that paper), so evidently trapped particles were not important in the mode damping, in seeming contradiction to the damping predicted by (50).

We will now show that (50), derived for an arbitrarily narrow partition squeeze, does not apply to the types of 'smooth' squeezes employed in Ashourvan and Dubin (2014). Rather than present a full theory of wave heating due to trapped particles in a smooth squeeze, we will find that useful results can be obtained from the following estimates.

A comparison of the second term in (39) (from which (50) is derived) and (106) of Ashourvan and Dubin (2014) shows a similar form for squeeze heating due to trapped and passing particles respectively, with the smooth squeeze passing particle Fourier coefficient α_m^n in Ashourvan and Dubin (2014) taking the place of the trapped particle coefficient C_n^l used here. The former coefficient α_m^n involves angle variable integrations (integrations over ψ) of the form $\int_0^{2\pi} d\psi \cos[k_m z[\psi]] \exp[in\psi]$, while the latter involves integrations only in position z (see (23)); but this difference arises only because the passing coefficient α_m^n is defined for squeezes with general functional forms in z where action-angle variables are required. We will take as a given that the theory of trapped particle heating in a general smooth squeeze potential also involves an angle variable Fourier coefficient similar to α_n^m. Then a theorem of Fourier analysis for smooth functions (see, for example, Boyd (1994)) implies that for large n the Fourier coefficient falls off exponentially, making a negligibly small contribution to the trapped particle heating sum in (39). This is as opposed to the behavior of the coefficients in a partition-type squeeze where $C_n^l \approx -m/4n^2$ for large n(see (A 2)). The exponential fall-off will occur roughly when n becomes larger than the spectral width of the function $\cos[k_m z(\psi)]$. Furthermore, for m of order unity we can estimate this spectral width to be of order $L/2\pi\Delta$ where Δ is the axial length scale of the squeeze; i.e. the Fourier coefficients of this function approach zero for $n \gtrsim L/2\pi\Delta$, assuming that $\Delta \ll L$. This follows because high n components of $z(\psi)$ arise from the rapid variation of the squeeze potential along the particle orbit. (The factor of 2π is an estimate obtained from examination of Fourier coefficients in squeeze potentials of various forms; somewhat different numerical coefficients can be obtained depending on exactly how one defines the spectral width.)

Now, the lower bound n_{min} on the sum in (39) is roughly $n_{min} \approx L\omega_m/2\pi v_s$. This bound is required simply in order for the resonances to fall in the trapped particle regime. However, when combined with the previous estimate of spectral width this implies that if $L\omega_m/v_s \gtrsim L/\Delta$, no terms in the sum contribute except those which are exponentially small and hence negligible. This is as opposed to the passing particle sum (see (106) of Ashourvan and Dubin (2014)) where the lower bound on the sum is m. This in turn implies that if the axial length scale Δ of the squeeze potential satisfies

$$\Delta \gtrsim v_s/\omega_m, \tag{51}$$

https://doi.org/10.1017/S0022377814000956 Published online by Cambridge University Press

trapped particle effects on the squeeze damping can be completely neglected, assuming that $\Delta \ll L$. While this is merely an estimate obtained from fairly crude scaling arguments, it does imply that for sufficiently small sufficiently smooth squeezes, the effect of trapped particles is not important to the squeeze damping. In particular, for Fig. 3 of Ashourvan and Dubin (2014) where $\Delta = 0.1L$ and $\varphi_s < T$, the inequality $\Delta > v_s/\omega_m$ is satisfied over the entire range of the figure. This explains why theory based only on passing particles was sufficient to explain the simulation results shown in the figure.

4. Collisional heating at the separatrix

In this section, we will add a weak collision effect to the system. Besides our analytical solutions, we use numerical methods to verify our results. We use the grids method to solve the differential equations related to the linearized, collisional Boltzmann equation, details of which are described in Appendix B. In a weakly collisional regime, small-angle scattering has the dominant collisional effect in scattering of particles in velocity space. In this regime the collisional effect is well-described by the Fokker–Planck collision operator given by:

$$C(f) = \frac{\partial}{\partial v}\left(D(v)\frac{\partial}{\partial v}f - \frac{v}{T}f\right) \tag{52}$$

$D(v)$ is the velocity space diffusion coefficient, which is a function of velocity. Since the Fokker–Planck collision operator contains derivatives of f with respect to v, the effects of collisions are significant in regions where these derivatives are large. The results from the previous section indicate that at the separatrix there is a discontinuity in f. Therefore, in the vicinity of the separatrix, derivatives of f become large and collisions significantly change the distribution function. Other regions in which collisions have significant effect due to large derivatives are the resonant regions.

The linearized Boltzmann equation with the Fokker–Planck collision operator describes the time evolution of the system:

$$\frac{\partial \delta \mathrm{f}}{\partial t} + v\frac{\partial \delta \mathrm{f}}{\partial z} - \frac{1}{m_q}\frac{\partial \delta\phi}{\partial z}\frac{\partial \mathrm{F}_0}{\partial v} = C(\delta \mathrm{f}). \tag{53}$$

We approximate the collision operator by its dominant term at the separatrix:

$$C(\delta f) \approx D(v)\partial_v^2 \delta f. \tag{54}$$

Using (8) and (9) in (53), for the time independent part of the linear distribution function and (10) for $\mathrm{F}_0(v)$ we obtain:

$$-i\omega_m \delta f + v\frac{\partial \delta f}{\partial z} + v\frac{\partial \delta\phi}{\partial z}\frac{\mathrm{F}_0}{T} = D(v)\partial_v^2 \delta f. \tag{55}$$

Considering that $\delta\phi(z)$ has an odd symmetry with respect to the center of plasma, the inherent symmetries of the solution to the above equation are:

$$\delta f(z, v) = -\delta f(-z, -v) \tag{56}$$

$$\delta f(z, v) = -\delta f(z + L, v). \tag{57}$$

In order to obtain a smooth and connected solution to δf at the separatrix, trapped and passing solutions must match at the separatrix $v = v_s$. We will solve for passing and trapped particles separately and match the solutions across the separatrix. Although the drive potential includes only a single harmonic drive with mode number

https://doi.org/10.1017/S0022377814000956 Published online by Cambridge University Press

m(see (5)), due to the collisions, the response of the plasma is not limited to the mth harmonic and has a series form

$$\delta f^p(z, v) = \sum_{\text{odd } m=-\infty}^{\infty} \delta f_m^p(v) e^{ik_m(z+L/2)} \tag{58}$$

Substituting from (5) in (55) we obtain

$$i(k_n v - \omega_m)\delta f_m^p + ik_m v \delta\phi_m^p \frac{\mathrm{F}_0}{T} = D(v)\frac{\partial^2 \delta f_m^p}{\partial v^2} \tag{59}$$

For the left and right trapped particles we substituting from (32) in (53) and obtain

$$i(k_{2n} v - \omega_m)\delta f_n^{l,r} + ik_{2n} v \delta\phi_n^{l,r} \frac{\mathrm{F}_0}{T} = D(v)\frac{\partial^2 \delta f_n^{l,r}}{\partial v^2} \tag{60}$$

The exact solution of these equations involve complex Airy functions and their integrals. We can use the boundary layer approximation method (Bender and Orszag 1978a) to find local solutions to these equations at the separatrix region. In the narrow separatrix layer the functions $\delta f_n^{l,r}$ and δf_m^p are rapidly varying, whereas all of the other functions of v present in (59) and (60) are slowly varying. We approximate all the slowly varying functions of v to be constants, with their values equal to their given value at $v = v_s$:

$$\mathrm{F}_0(v) \approx \mathrm{F}_0(v_s) \tag{61}$$

$$D(v) \approx D(v_s) \tag{62}$$

$$(k_m v - \omega_m)\delta f_m^p \approx (k_m v_s - \omega_m)\delta f_m^p \tag{63}$$

$$(k_{2n} v - \omega_m)\delta f_n^{l,r} \approx (k_{2n} v_s - \omega_m)\delta f_n^{l,r} \tag{64}$$

In order for the approximations in (63) and (64) to be correct, i.e. the variation of the functions $(k_m v - \omega_m)$ and $(k_{2n} v - \omega_m)$ to be small compared to their value at the separatrix, the resonant regions for which $v_n \approx \omega_m / k_{2n}$ for trapped, and $v_m \approx \omega_m / k_m$ for passing region, must be far from the sparatrix layer. Hence, the following condition must be satisfied:

$$\Delta_n^{\mathrm{res}} + \Delta_n^s \ll |v - \omega_m / k_n|, \tag{65}$$

where Δ_n^s is the width of the separatrix layer and Δ_n^{res} is the width of nth resonance. In the collisionless theory resonances are singularities in the velocity space and have zero width. However, introducing collisions into the system broadens these resonances and we represent the width of the nth resonance with Δ_n^{res}. Equation (65) dictates the condition that the resonance regions and the separatrix boundary layer must not overlap. In other words, regions of rapid variation of the solutions must be isolated.

The approximate differential equation in the passing region of the boundary layer is given by

$$i(k_m v_s - \omega_m)\delta f_m^p + ik_m v \delta\phi_m^p \frac{\mathrm{F}_0(v_s)}{T} = D(v_s)\frac{\partial^2 \delta f_m^p}{\partial v^2} \tag{66}$$

This equation has a particular solution which is given by

$$\delta f_m^p = \frac{\delta\phi_m^p v_s \mathrm{F}_0(v_s)/T}{\omega_m / k_m - v_s} \tag{67}$$

https://doi.org/10.1017/S0022377814000956 Published online by Cambridge University Press

This solution corresponds to the collisionless solution (30), evaluated at the separatrix $v = v_s$. The homogeneous solutions to (66) are given by

$$\delta f_m^p = \delta\phi_m^p \frac{\mathrm{F}_0(v_s)}{T} a_m^{\pm} \exp[\pm i^{3/2}\sqrt{(\omega_m - k_m v_s)/D}(v - v_s)]. \tag{68}$$

Since we expect the solutions to stay finite as $v \to +\infty$, the only acceptable solution for the passing region will be the plus sign and we take $a_m^+ = a_m$. Using (67) and (68), the total solution inside the passing region of the separatrix layer is given by

$$y_{\mathrm{in}}(v) = \frac{\delta\phi_m^p v_s \mathrm{F}_0(v_s)/T}{\omega_m/k_m - v_s} + \delta\phi_m^p \frac{\mathrm{F}_0(v_s)}{T} a_m \exp[i^{3/2}\sqrt{(\omega_m - k_m v_s)/D}(v - v_s)], \tag{69}$$

which has an undetermined coefficient, a_m. This coefficient, together with all the other undetermined coefficients from the trapped region, will be determined from matching the boundary values at the separatrix. The first term on the right-hand side is the contribution from the collisionless system. The second term on the right-hand side is the perturbation to the collisionless solution, due to the effect of collisions. This solution falls to zero rapidly in a region with a thickness approximately given by

$$\Delta_m^s = \sqrt{2D/(\omega_m - k_m v_s)}, \tag{70}$$

which is the inverse of the coefficient of real part of the exponent in (69).

The boundary layer, which is characterized by the rapid variation of solutions, connects to the passing region far from the separatrix, which we call the outer region. In the outer region, the solution to (59) varies slowly and the derivatives of δf_m^p are small. Since the system is weakly collisional and $D(v)$ is small, we can take $D(v)\partial^2\delta f/\partial v^2 \approx 0$ in the outer region. As the result of this approximation, the outer region solution to (59) will be:

$$y_{\mathrm{out}}(v) = \frac{\delta\phi_m^p v \mathrm{F}_0(v)/T}{\omega_m/k_m - v}, \tag{71}$$

which is identical to collisionless passing region solution in (30).

So far we have the solution for δf_m^p within the boundary layer given by equation (69), which we called $y_{\mathrm{in}}(v)$, and the solution for the outer region, given by (71), which we called $y_{\mathrm{out}}(v)$. In order to connect these two solutions and obtain a uniform solution over v, we compare the asymptotic form of $y_{\mathrm{in}}(v)$ and $y_{\mathrm{out}}(v)$ to obtain a solution describing the middle region, i.e. between outer and inner solutions:

$$\begin{aligned} \lim_{v\to\infty} y_{\mathrm{in}}(v) &= \frac{\delta\phi_m^p v_s \mathrm{F}_0(v_s)/T}{\omega_m/k_m - v_s}, \\ \lim_{v\to v_s} y_{\mathrm{out}}(v) &= \frac{\delta\phi_m^p v_s \mathrm{F}_0(v_s)/T}{\omega_m/k_m - v_s}. \end{aligned} \tag{72}$$

Therefore, we take the middle region solution to be:

$$y_{\mathrm{mid}}(v) = \frac{\delta\phi_m^p v_s \mathrm{F}_0(v_s)/T}{\omega_m/k_m - v_s} \tag{73}$$

We can define a uniform solution as follows:

$$y_{\mathrm{uniform}}(v) = y_{\mathrm{in}}(v) + y_{\mathrm{out}}(v) - y_{\mathrm{mid}}(v). \tag{74}$$

https://doi.org/10.1017/S0022377814000956 Published online by Cambridge University Press

Substituting from (69), (71) and (73) into (74), we obtain a uniform solution for the passing region distribution function δf_m^p:

$$\delta f_m^p(v) = \frac{\delta\phi_m^p v \mathrm{F}_0(v)/T}{\omega_m/k_m - v} + \delta\phi_m^p \frac{\mathrm{F}_0(v_s)}{T} a_m \exp[i^{3/2}\sqrt{(\omega_m - k_m v_s)/D}(v - v_s)]. \tag{75}$$

As the effect of collisions become weaker, D decreases and the boundary layer shrinks. In the limit where D goes to zero, the boundary layer vanishes and we retrieve the collisionless solution at separatrix from the first term in (75).

Following the steps taken for the passing region, a uniform boundary layer solution to (60) for the left trapped particles is given by

$$\delta f_n^l = \frac{\delta\phi_n^l v \mathrm{F}_0(v)/T}{\omega_m/k_{2n} - v} + \delta\phi_n^l \frac{\mathrm{F}_0(v_s)}{T} b_n \exp[-i^{3/2}\sqrt{(\omega_m - k_{2n} v_s)/D}(v - v_s)]. \tag{76}$$

The first term on the right-hand side is the collisionless solution and the second term is the correction due to collisions and we took the negative sign in order for the solution to stay finite as $v \to 0$. The undetermined coefficient b_n is found by matching the solutions at the separatrix. Due to symmetry, the right trap solutions are redundant and contain no extra information. The boundary layer thickness for the nth trapped Fourier component is defined as

$$\Delta_{2n}^s = \sqrt{2D/(\omega_m - k_{2n} v_s)} \tag{77}$$

As was the case for the passing solutions, boundary thickness, which is proportional to $\sqrt{D}$, vanishes as D goes to zero and the collisionless solution will be retrieved. Therefore in the presence of weak collisions, the separatrix is surrounded by a layer of width proportional to $\sqrt{D}$ from both above and below v_s.

4.1. *Matching the boundary solutions at separatrix*

By matching the solutions obtained for trapped and passing distribution functions, we obtain a uniform solution over the whole separatrix region in (z, v) phase space. The passing distribution has the functional form given by (27) with δf_m^p given by (75). We expand the functions $e^{ik_m(z+L/2)}$ in terms of the complete set of functions $e^{ik_{2n}z}$ which have L periodicity:

$$e^{ik_m(z+L/2)} = \sum_{n=-\infty}^{\infty} l_n^m e^{ik_{2n}z}, \quad l_n^m = \frac{1}{L}\int_{-L}^{0} e^{i(k_m - k_{2n})z} dz$$

$$l_n^m = \frac{\sin\frac{m\pi}{2}}{\pi(n - m/2)}, \text{ m odd} \tag{78}$$

As a result, we can rewrite the passing distribution given in (58) as

$$\delta f^p(z, v) = \sum_{n=-\infty}^{\infty} \left(\sum_{\text{odd } m=-\infty}^{\infty} l_n^m \delta f_m^p \right) e^{ik_{2n}z} \tag{79}$$

Comparing the above equation to (32), the matching conditions at the separatrix for the left half of the plasma are given by

$$\begin{pmatrix} \delta f_n^l(v_s) \\ \frac{\partial \delta f_n^l(v_s)}{\partial v} \end{pmatrix} = \sum_{\text{odd } m=-\infty}^{\infty} l_n^m \begin{pmatrix} \delta f_m^p(v_s) \\ \frac{\partial \delta f_m^p(v_s)}{\partial v} \end{pmatrix} \tag{80}$$

https://doi.org/10.1017/S0022377814000956 Published online by Cambridge University Press

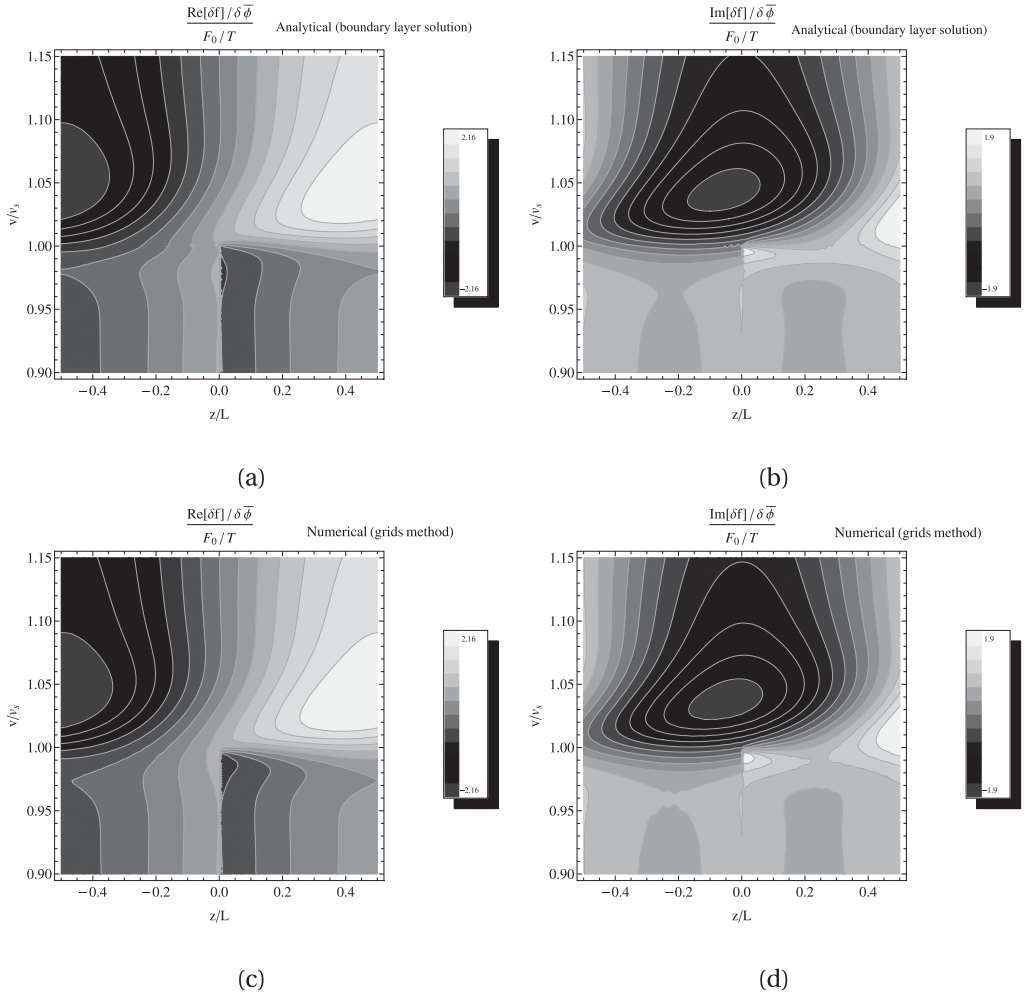


FIGURE 6. Contour plots of the real and imaginary part of δf in the z, v phase space, near the separatrix ($v/v_s \approx 1$), for $v_T/v_s = 1.73$ and for diffusion coefficient $DL/v_s^3 = 2 \times 10^{-4}$. Plots (a) and (b) are obtained from the analytical boundary layer method and plots (c) and (d) are obtained from the numerical grids method.

For the right half of plasma we use the symmetry relation (56). We substitute the boundary layer solutions, (76) for δf_n^l and (69) for δf_m^p, in the sets of equations in (80) and solve them to determine the unknown coefficients, a_m (passing) and b_n (trapped). The coefficients are functions only of $\omega_m/k_m v_s$, since we factored out their dependence on T which was of the form $\mathrm{F}_0(v_s)/T$. For the purpose of practicality we need to truncate the infinite series in order to evaluate the unknown coefficients. Keeping M terms on the trapped side implies there are $2M$ equations, so we need to keep M terms on the passing side so as to have the same number of equations as unknowns.

Using Mathematica, we solve for the unknown coefficients a_m and b_n. Figure 6 compares the contour plots of the time independent part of the distribution function δf in the vicinity of the separatrix $v \sim v_s$ over the (z, v) phasespace, for mode $m = 1$ drive potential, with $v_T/v_s = 1.73, \omega_m/k_1 v_s = 0.8$, and diffusion constant $DL/v_s^3 = 2\times 10^{-4}$. $M = 101$ terms are kept for trapped particles ($n = -50, -49, \ldots, 49, 50$) and $M = 101$ for passing ($m = -101, -99, \ldots, 97, 99$) in the matching equations, (80).

https://doi.org/10.1017/S0022377814000956 Published online by Cambridge University Press

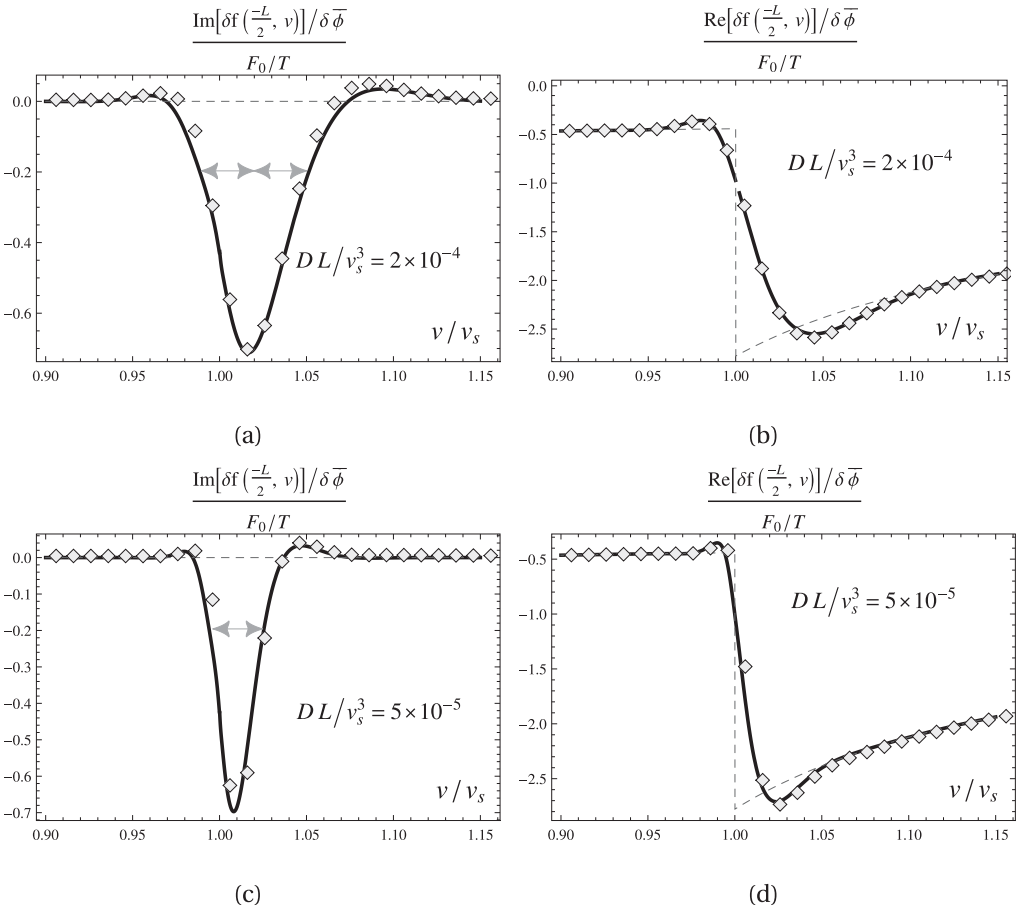


FIGURE 7. Plots of the real and imaginary part of δf as a function of v/v_s near the separatrix ($v/v_s \approx 1$), at the left end of plasma $z = -L/2$, for $v_T/v_s = 1.73$ and for diffusion coefficient given by $DL/v_s^3 = 2 \times 10^{-4}$ and $DL/v_s^3 = 5 \times 10^{-5}$. Solid curves are obtained analytically via the boundary layer method. Dashed lines are the collisionless solutions. Numerical grids method results are depicted in diamonds. Double-headed arrows show the width of separatrix layer. Dashed lines show collisionless theory.

In Fig. 7, $\delta f(z, v)$ is plotted near the separatrix, at the left end of plasma $z = -L/2$, for the same parameters as Fig. 6, as well as for $DL/v_s^3 = 5 \times 10^{-5}$. The results from the numerical grids method are plotted in diamonds. The dashed curve shows the δf from the collisionless theory. As shown by the arrows, the width of the separatrix layer for plot (c) is approximately two times smaller than the width of the separatrix layer in the plot (a), consistent with the expected $\sqrt{D}$ dependence of the width of the separatirx layer.

Now that we have obtained the collisional δf_m^p and δf_n^l , we can calculate the heating at separatrix. For sufficiently small D, away from resonances, the separatrix layer can be considered as an isolated region. Heating in separatrix can then be calculated independently and added to the resonant heating in other parts of phase space to get the total heating.

We substitute the solved collisional δf_n's in the average heating (39) and perform the integrals. At $v \approx v_s$, the first term of δf_m^p and δf_n^l, given by (75) and (76) are purely real and give the collisionless solutions. As a result, they do not contribute to

https://doi.org/10.1017/S0022377814000956 Published online by Cambridge University Press

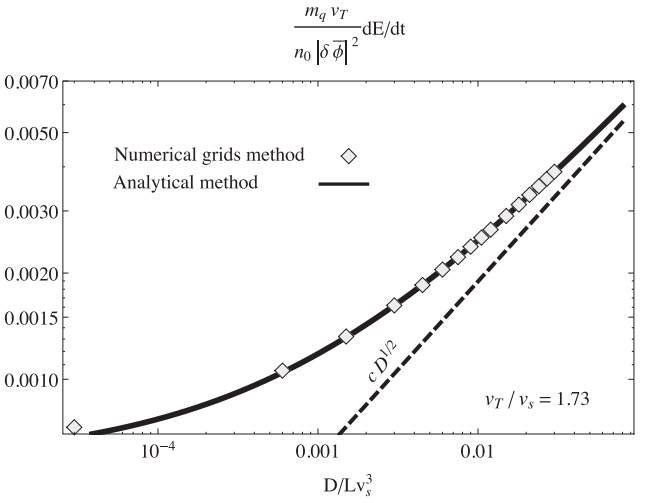


FIGURE 8. Heating per unit time versus the diffusion coefficient D, for $v_T/v_s = 1.73$ and $\omega_m/k_1 v_s = 0.2$ and for drive mode $m = 1$. The dashed line depicts a $\sqrt{D}$ dependence for comparison.

heating integrals. The second term which is the collisional correction to δf_m^p and δf_n^l has non-zero value in the integral which is equal to:

$$\frac{dE_{\rm sep}^p}{dt} = n_0 L \sum_{m=-\infty}^{\infty} k_m \mathrm{F}_0(v_s) \frac{|\delta\overline{\phi}|^2}{T} \mathrm{Re}\left(a_m \left[-v_s i^{-1/2} \sqrt{\frac{D}{\omega_m - k_m v_s}} + i^{-2} \frac{D}{\omega_m - k_m v_s} \right] \right), \tag{81}$$

for the passing side of the separatrix layer, and

$$\frac{dE_{\rm sep}^t}{dt} = 2n_0 L \sum_{n=-\infty}^{\infty} k_{2n} (C_n^l)^2 \mathrm{F}_0(v_s) \frac{|\delta\overline{\phi}|^2}{T} \mathrm{Re} \times \left(b_n \left[v_s i^{-1/2} \sqrt{\frac{D}{\omega_m - k_{2n} v_s}} - i^{-2} \frac{D}{\omega_m - k_{2n} v_s} \right] \right), \tag{82}$$

for the trapped side of separatrix, which has a factor of two in order to include the heating from both right and left sides. In evaluation of (82), the limits of integration was from zero to v_s, but the lower limit of integral has been taken to be $-\infty$, since δf falls to zero on the scale of separatrix layer thickness which is much smaller than v_s. The total heating in the separatrix layer is subsequently equal to the sum of the heating in the passing (81) and trapped (82) side of the separatrix:

$$\frac{dE_{\rm sep}}{dt} = \frac{dE_{\rm sep}^p}{dt} + \frac{dE_{\rm sep}^t}{dt} \tag{83}$$

Although weak collisions broaden the resonance regions, the change in resonant heating due to these weak collisions is negligible. As a result the total heating of the plasma is the sum of the separatrix heating and the collisionless resonant heating obtained in (39).

In Fig. 8, dE/dt is plotted versus the diffusion coefficient D, for $v_T/v_s = 1.73$ and $\omega_m/k_1 v_s = 0.2$ and for drive mode $m = 1$. At this frequency the resonances are far from the separatrix and therefore, the separatrix layer is isolated, thus theory is

https://doi.org/10.1017/S0022377814000956 Published online by Cambridge University Press

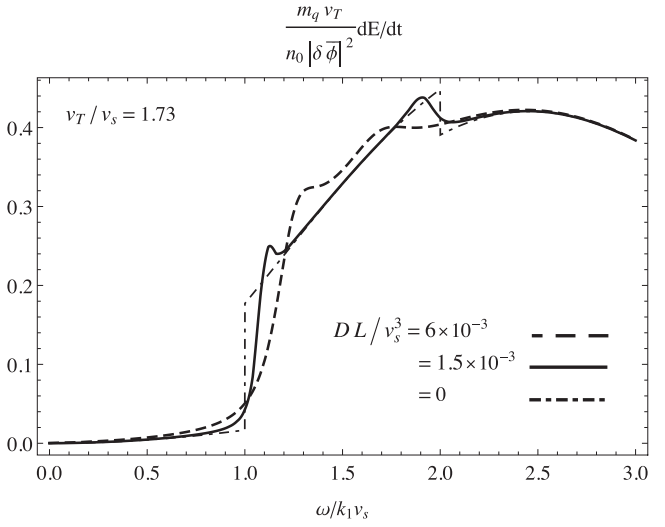


FIGURE 9. Heating per unit time as a function of ω_m, obtained from numerical grids method for $D = 1.5 \times 10^{-3}$, and $D = 6 \times 10^{-3}$, and obtained from (39) for $D = 0$.

expected to work well. The results obtained from the numerical grids method are depicted in diamonds and the analytically obtained heating is depicted in a solid curve. As $D \to 0$ the value of the dE/dt tends to the collisionless heating obtained from (39). Furthermore, as D grows the heating at the separatrix layer dominates. This heating has a $\sqrt{D}$ dependence.

Figure 9 depicts the heating versus the drive frequency ω_m. Heating for a collisionless plasma ($D = 0$) is depicted in a dash-dotted curve and evaluated using (39). The collisional heating result is obtained from the numerical grids method and depicted in a solid curve for $D = 1.5 \times 10^{-3}$, and a dashed curve for $D = 6 \times 10^{-3}$. The collisionless heating is discontinuous for two values of frequency. At $\omega_m/k_1 v_s = 1$ the passing resonance appears at the separatrix velocity v_s, which causes a discontinuous jump in the collisionless heating curve. At $\omega_m/k_1 v_s = 2$ the $n = 1$ trapped resonance disappears at the separatrix and this causes a sudden drop at in the collisionless heating curve. In the presence of collisions, the added heating at the separatrix connects and smooths out these discontinuities, as we can see from the plots related to $D = 1.5 \times 10^{-3}$ and $D = 6 \times 10^{-3}$.

In Figs 10(a) and (b) we compare the heating obtained from the analytical boundary layer method and depicted in diamonds, to the numerical grids method results depicted in solid curves, for the same parameters as Fig. 9. The dashed curves show the collisionless heating for comparison purposes. For the smaller value of D we have a better agreement between the two methods. Furthermore, we can see that as the frequencies approach resonance, at $\omega_m/k_1 v_s = 1$ in Fig. 10(a) and at $\omega_m/k_1 v_s = 2$ in Fig. 10(b), the analytical results deviate from the numerical results. Since the separatrix layer and resonance regions are overlapping the boundary layer theory is no longer valid.

Figure 11 depicts the heating for larger values of the drive frequency ω_m. At large values of $\omega_m/k_m v_s$ the discontinuity in the distribution function between the trapped and passing regions becomes small and as a result the collisional heating due to the separatrix is not a large effect. Instead, collisions simply smooth out the steps in the heating rate caused by the disappearance of resonances in the trapped particle

https://doi.org/10.1017/S0022377814000956 Published online by Cambridge University Press

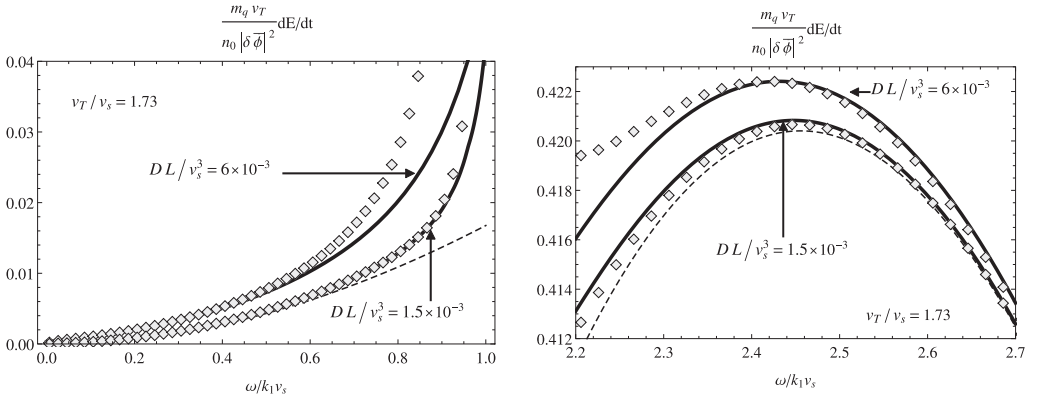


FIGURE 10. Heating per unit time as a function of ω_m. The results from the analytical boundary layer method are depicted in diamonds. The numerical grids method results are depicted in solid curves. The dashed line is collisionless theory.

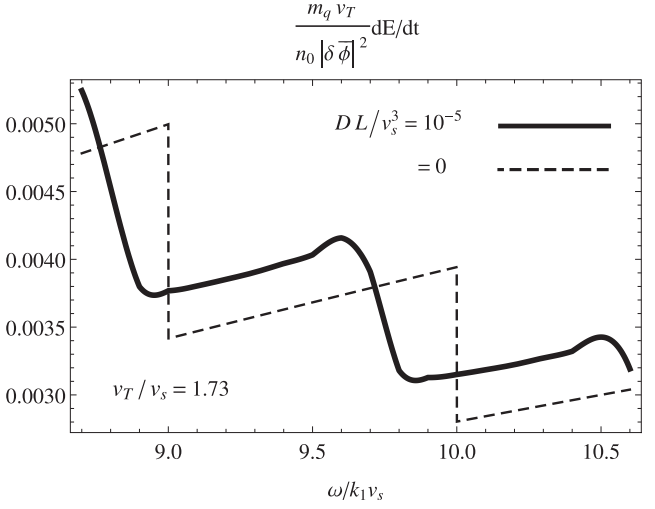


FIGURE 11. Heating per unit time as a function of ω_m.

distribution as ω_m increases. For large wave phase velocities, passing and trapped particles near the separatrix energy have nearly the same response to the wave, so the separatrix discontinuity is small and not important to the wave heating. This is as opposed to small wave phase velocities, where there is a large discontinuity in the distribution function at the separatrix and hence a dominant collisional separatrix heating effect.

5. Conclusion

We have presented a 1D model of a finite length plasma with its population divided in velocity space into passing particles with $|v| > v_s$ and trapped particles with $|v| < v_s$. The squeeze potential that creates this division is assumed for simplicity to be an infinitesimally narrow kinetic barrier of amplitude $\varphi_s = \frac{1}{2}m_q v_s^2$. We then apply a standing sinusoidal drive potential of odd symmetry with respect to the center

https://doi.org/10.1017/S0022377814000956 Published online by Cambridge University Press

of plasma. Consequently, passing and trapped particles experience different perturbed potentials along their unperturbed orbits. The response of the trapped particles to the external drive is non-sinusoidal and contains higher harmonics while passing particles are unaffected by the narrow barrier.

The 1D model used here neglects radial variation of the squeeze and drive potentials, and so the results only provide qualitative information as to the size of the heating effects due to squeeze, as opposed to a more realistic model (Ashourvan and Dubin 2014) that includes radial inhomogeneity of the plasma. Nevertheless, we are able to draw several conclusions from the analysis based on this 1D model:

(i) The drive potential performs non-zero average work on the resonant particles due to a series of higher harmonics in the trapped region at bounce frequencies $\omega_b(E_n) = \omega_m/n$. In the regime where $\omega_m/k_m v_T \gg 1$, and for the narrow squeeze barrier considered here, the resonant heating in the passing region is exponentially small, and the sum of the trapped particle resonant contributions results in finite collisionless heating of the plasma. Thus, trapped particles dominate the enhanced heating due to squeeze in this model.

(ii) For a smooth squeeze of finite axial width Δ, we estimate that the trapped particle contribution to the enhanced collisionless heating arising from squeeze becomes negligible compared to the passing particle contribution when Δ satisfies $\Delta \gtrsim v_s/\omega_m$. Hence, trapped particles are important for collisionless squeeze damping due to the narrow squeeze considered here (with $\Delta = 0$), but for the small ($v_s < v_T$) smooth squeezes considered in Ashourvan and Dubin (2014) trapped particles have negligible impact on the damping.

(iii) The collisionless particle velocity distribution function is discontinuous at the separatrix ($v = v_s$) because trapped and passing particles respond differently to the drive potential. Adding weak collisions in the form of a Fokker–Planck collision operator results in large correctional terms at the separatrix. These corrections connect and smooth out the passing and trapped solutions at the separatrix. Furthermore, the drive potential performs non-zero work in the separatrix layer which can add large contributions to the heating, scaling as $\sqrt{D}$, in the regime where $\omega_m/k_m v_s \leqslant 1$ (where D is the velocity diffusion coefficient). However, when $\omega_m/k_m v_s \gg 1$ the discontinuity at the separatrix becomes small and collisionless heating due to Landau resonances caused by the squeeze is the dominant effect. This is because the response of particles at or near the separatrix velocity no longer depends on whether they are trapped or passing when the wave phase velocity is large, since such particles move axially only a small fraction of the plasma length in a wave period. Hence, for the high-phase-velocity weakly-damped modes considered in Ashourvan and Dubin (2014), enhanced collisional effects associated with the separatrix boundary layer can be neglected.

Thus, the work presented here indicates that the perturbative collisionless theory of Ashourvan and Dubin (2014) should be sufficient to describe the results of ongoing experiments that apply small smooth squeeze potentials to weakly collisional cylindrical non-neutral plasma columns, and that observe enhanced TG mode damping. The results of such experiments will be presented in a future paper.

Nevertheless, several issues remain to be addressed. For instance, in the drive regime $\omega_m/k_m v_s \leqslant 1$ we found that heating from the collisional boundary layer is important and trapped particle effects on the heating are also important. However, in this regime the collective plasma response is closer to a Debye-shielding response than to the axially-sinusoidal plasma mode considered here, and this collective response should

https://doi.org/10.1017/S0022377814000956 Published online by Cambridge University Press

be properly accounted for. Such self-consistent effects on low-frequency collisional heating will be considered in future work. Also, we consider here only azimuthally-symmetric plasma modes. However, for modes with azimuthal dependence there is an $\mathbf{E}\times\mathbf{B}$ drift response to the plasma wave due to the azimuthal wave electric field. This $\mathbf{E}\times\mathbf{B}$ drift response could produce a discontinuity at the separatrix even for large axial phase velocities, possibly resulting in strong boundary layer heating at the separatrix even for $\omega_m/k_m v_s \gg 1$. This could explain experimental results such as those observed in Kabantsev and Driscoll (2006). These issues will be addressed in future work.

Acknowledgements

This work is supported by NSF grant number PHY0903877 and DOE grant number DE-SC0002451.

Appendix A. Collisionless heating for $\omega_m/k_m v_T \gg 1$

In the large frequency limit the heating due to passing particle resonance is exponentially small, thus the plasma heating is due to the trapped resonances:

$$\frac{dE}{dt} = \pi L n_0 \frac{|\delta\bar{\phi}|^2}{T} \sum_{n'=n_{\min}}^{\infty} k_{2n'} |C^l_{n'}|^2 v^2 \mathrm{F}_0(v)|_{v=\frac{\omega}{k_{2n'}}}, \quad n_{\min} = \lceil \tfrac{\omega}{k_2 v_s} \rceil \tag{A 1}$$

For $n_{\min} \gg 1$, from (25) we can approximate:

$$C^l_n \approx -\frac{m}{4n^2} \tag{A 2}$$

Defining the drive frequency $f = \omega_m/2\pi$, the trapped heating in the large frequency limit, substituting for F_0 from (10), in the limit $\omega_m/k_m v_T \gg 1$ can be written as

$$\frac{dE}{dt} = \sqrt{\frac{2}{\pi}} \frac{n_0}{m_q} |\delta\bar{\phi}|^2 \sum_{n'=\lceil \frac{Lf}{v_s} \rceil}^{\infty} \frac{L^2 f^2}{v_T^3} \frac{m^2}{4(n')^5} \exp\left(-\frac{f^2 L^2}{2(n')^2 v_T^2}\right) \tag{A 3}$$

We perform the change of dummy variable n' to $n + \lceil \frac{Lf}{v_s} \rceil$, and since $\frac{Lf}{v_s}$ is large, in the argument of the sum we substitute $\lceil \frac{Lf}{v_s} \rceil$ with $\frac{Lf}{v_s}$ to obtain:

$$\begin{aligned} \frac{dE}{dt} &= \sqrt{\frac{2}{\pi}} \frac{n_0}{m_q} |\delta\bar{\phi}|^2 \frac{m^2}{4v_T^3} \sum_{n=0}^{\infty} \frac{L^2 f^2}{(n + \frac{Lf}{v_s})^5} \exp\left(-\frac{f^2 L^2}{2(n + \frac{Lf}{v_s})^2 v_T^2}\right) \\ &= \sqrt{\frac{2}{\pi}} \frac{n_0}{m_q} |\delta\bar{\phi}|^2 \frac{m^2}{4v_T^3} \frac{v_s^4}{L^2 f^2} S(v_s/v_T), \end{aligned} \tag{A 4}$$

where we defined

$$S(v_s/v_T) = \sum_{n=0}^{\infty} \frac{1}{(1+t_n)^5} e^{-\frac{(v_s/v_T)^2}{2(1+t_n)^2}} (t_{n+1} - t_n) \tag{A 5}$$

$$t_n = \frac{n v_s}{Lf} \tag{A 6}$$

https://doi.org/10.1017/S0022377814000956 Published online by Cambridge University Press

In the limit $\frac{Lf}{v_s} \to \infty$ we have $t_{n+1} - t_n = 1/\frac{Lf}{v_s} \to 0$, the above sum can be approximated by the Riemann integral as follows (Bender and Orszag 1978b)

$$S(f) = \int_0^\infty \frac{1}{(1+t)^5} e^{-\frac{(v_s/v_T)^2}{2(1+t)^2}} dt = \int_0^1 u^3 e^{-(\frac{v_s}{v_T})^2 \frac{u^2}{2}} du$$
$$= 2\left(\frac{v_T}{v_s}\right)^4 \left[1 - \left(1 + \frac{1}{2}\left(\frac{v_s}{v_T}\right)^2\right) e^{-\frac{1}{2}\left(\frac{v_s}{v_T}\right)^2}\right] \tag{A 7}$$

Thus, in the limit of large frequencies for which $\omega_m/k_m \gg v_T$, we have

$$\frac{dE}{dt} = 2\sqrt{\frac{2}{\pi}} \frac{n_0}{m_q} |\delta\overline{\phi}|^2 \frac{v_T}{v_{ph}^2} \left[1 - \left(1 + \frac{1}{2}\left(\frac{v_s}{v_T}\right)^2\right) e^{-\frac{1}{2}\left(\frac{v_s}{v_T}\right)^2}\right], \quad \omega_m/k_m v_T \gg 1 \tag{A 8}$$

where $v_{ph} = \omega_m/k_m$ is the wave phase velocity. In the limit where $v_s/v_T \gg 1$, the exponential term in (A 8) will tend to zero. Therefore the heating will be of the form

$$\frac{dE}{dt} = \frac{2n_0|\delta\overline{\phi}|^2}{m_q} \sqrt{\frac{2}{\pi}} \frac{v_T}{v_{ph}^2} \tag{A 9}$$

In the limit where $v_s/v_T \ll 1$, we expand the exponential in A 8 to obtain

$$\frac{dE}{dt} = \frac{2n_0|\delta\overline{\phi}|^2}{m_q} \sqrt{\frac{2}{\pi}} \frac{v_T}{v_{ph}^2} \left[1 - \left(1 + \frac{v_s^2}{2v_T^2}\right)\left(1 - \frac{v_s^2}{2v_T^2} + \frac{v_s^4}{8v_T^4} + \cdots\right)\right]$$
$$\approx \frac{n_0|\delta\overline{\phi}|^2}{m_q} \sqrt{\frac{2}{\pi}} \frac{v_s^4}{4v_{ph}^2 v_T^3} \tag{A 10}$$

In summary, we have:

$$\frac{dE}{dt} = \frac{2n_0|\delta\overline{\phi}|^2}{m_q} \sqrt{\frac{2}{\pi}} \frac{v_T}{v_{ph}^2}, \quad v_{ph} \gg v_s \gg v_T \tag{A 11}$$
$$= \frac{n_0|\delta\overline{\phi}|^2}{m_q} \sqrt{\frac{2}{\pi}} \frac{v_s^4}{4v_{ph}^2 v_T^3}, \quad v_{ph} \gg v_T \gg v_s \tag{A 12}$$

Appendix B. Numerical grids method

We use the grids method to numerically solve for the linear distribution of finite length plasma with weak collisions and an applied squeeze which is infinitesimally narrow. We solve the following linearized Boltzmann equation to obtain the time independent part of the linear distribution function $\delta f(z, v)$ define in (9)

$$-i\omega\delta f + v\frac{\partial \delta f}{\partial v} + \frac{v}{T}\delta\varphi(z)\mathrm{F}_0(v) = D\frac{\partial}{\partial v}\left(\frac{\partial \delta f}{\partial v} + \frac{v}{T}\delta f\right) \tag{B 1}$$

where $\delta\varphi(z)$ is given by (5) and the diffusion coefficient D is taken to be a constant in all phase space. The above equation is a PDE in z and v. We can discretize these independent variables in the above equation and solve for δf on a coarse-grained (z, v) phasespace. Grid point position coordinates in phase space are given by

$$z_n = n\Delta z - z_0, \quad n = -N+1, \ldots, N \tag{B 2}$$
$$v_m = m\Delta v - v_0, \quad m = -M+1, \ldots, M$$

https://doi.org/10.1017/S0022377814000956 Published online by Cambridge University Press

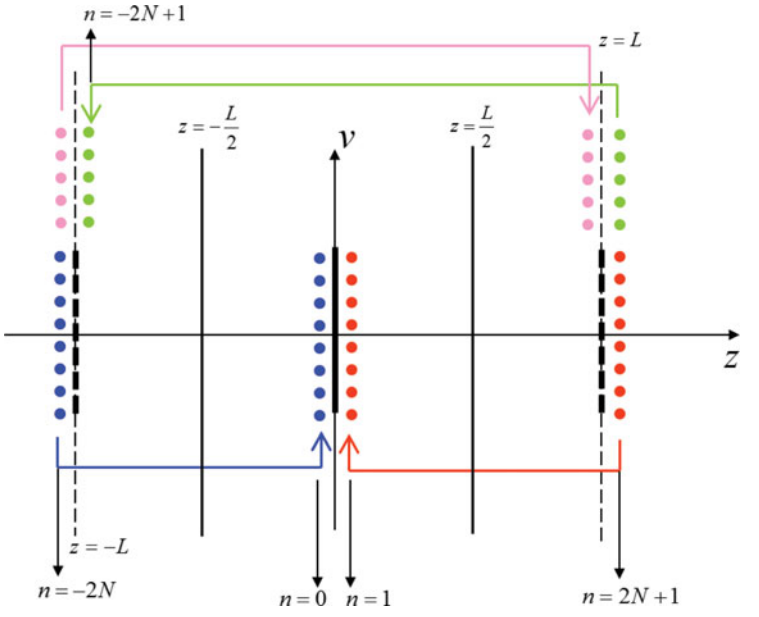


FIGURE 12. Enforcing the periodic boundary condition on the grid point solutions outside the extended phase space.

where $\Delta z = L/(2N)$ and $\Delta v = V_{\max}/M$ are the stepsizes between grid points in position and velocity space, $z_0 = \Delta z/2$ and $v_0 = \Delta v/2$. At a constant velocity v_m, there are equal number of grid points $N/2$ on the left and right side of $z = 0$. The leftmost of which is $z_{-N+1} = -L + \Delta z/2$, which is the closest part of plasma near the left wall, and the right-most of which is $z_N = L - \Delta z/2$, closest the plasma gets to the right wall. $V_{\max}$ is an arbitrary velocity magnitude at which we approximate the value of δf to be given by the collisionless solution in (31), which must be far enough from the separatrix or resonances such that the boundary solution does not affect the solutions in the aforementioned regions.

Axial boundary conditions on the left and right wall and on the squeeze are all specular, given by (3) and (38)

Based on these boundary condition we construct the extended coarse-grained phase space. Figure 12 describes the grid boundary postitions and enforcing the boundary conditions which relate the value of δf at different grid points.

The linear PDE in (B 1) must become discretized by replacing all the partial derivatives with their discrete form, which we choose to be centered difference:

$$\begin{aligned}
\frac{\partial \delta f(z_n, v_m)}{\partial z} &= \frac{\delta f(z_n + \Delta z, v_m) - \delta f(z_n - \Delta z, v_m)}{2\Delta z} \\
&= \frac{\delta f(z_{n+1}, v_m) - \delta f(z_{n-1}, v_m)}{2\Delta z} \\
\frac{\partial \delta f(z_n, v_m)}{\partial v} &= \frac{\delta f(z_n, v_m + \Delta v) - \delta f(z_n, v_m - \Delta v)}{2\Delta v} \\
&= \frac{\delta f(z_{n+1}, v_{m+1}) - \delta f(z_n, v_{m-1})}{2\Delta v} \\
\frac{\partial^2 \delta f(z_n, v_m)}{\partial v^2} &= \frac{\delta f(z_n, v_{m+1}) - 2\delta f(z_n, v_m) + \delta f(z_n, v_{m-1})}{\Delta v^2}
\end{aligned} \tag{B 3}$$

https://doi.org/10.1017/S0022377814000956 Published online by Cambridge University Press

Replacing the discrete derivatives in (B 1), this equation is transformed into a series of coupled, linear equations for $\delta f(z_n, v_m)$. There is an equation for each point inside the (extended) phase space. We solve these equations over the constructed phase space and its related boundary conditions. In the next step, the discrete solution is interpolated over the 2D phase space to get a smooth and continuous solution. Furthermore, using (38) we can use the obtained $\delta f(z, v)$ to calculate the heating per unit time.

REFERENCES

Anderson, M. W. and O'Neil, T. M. 2007 *Phys. Plasmas* **14**, 112 110.

Ashourvan A. and Dubin, D. H. E. 2014 *Phys. Plasmas* **21**, 052 109.

Bender, C. M. and Orszag, S. A. 1978a *Advanced Mathematical Methods for Scientists and Engineers*, McGraw-Hill, ch. 9.

Bender, C. M. and Orszag, S. A. 1978b *Advanced Mathematical Methods for Scientists and Engineers*, McGraw-Hill, ch. 6, pp. 302–304.

Boyd, J. P. 1994 *J. Comput. Phys.* **110**, 360.

Danielson, J. R., Anderegg, F. and Driscoll, C. F. 2004 *Phys. Rev. Lett.* **92**, 245 003.

Driscoll, C. F., Kabantsev, A. A. and Dubin, D. H. E. 2013 Transport, damping, and wave-couplings from chaotic and collisional neoclassical transport, in non-neutral plasma physics VIII. *AIP Conf. Proc.* **1521**, 15.

Dubin, D. H. E. and Tsidulko, Y. A. 2011 *Phys. Plasmas* **18**, 062 114.

Hilsabeck, T. J. and O'Neil, T. M. 2003 *Phys. Plasmas* **10**, 3492.

Kabantsev, A. A. and Driscoll, C. F. 2006 *Phys. Rev. Lett.* **97**, 095 001.

Krall, N. A. and Trivelpiece, A. W. 1986 "Principles of Plasma Physics", San Francisco Press, p. 376.

Prasad, S. A. and O'Neil, T. M. 1983 *Phys. Fluids* **26**, 665.

Stix, T. H. 1962 *The Theory of Plasma Waves*, McGraw-Hill.

Trivelpiece, A. W. and Gould, R. W. 1959 *J. Appl. Phys.* **30**, 1784.

https://doi.org/10.1017/S0022377814000956 Published online by Cambridge University Press